

# Impact of Water Ingress on Molybdenum thin films and its effect on Cu(In,Ga)Se<sub>2</sub> Solar Cells

Shankar Karki<sup>1</sup>, Julia I. Deitz<sup>2</sup>, Grace Rajan<sup>1</sup>, Sina Soltanmohammad<sup>3</sup>, Deewakar Poudel<sup>1</sup>, Benjamin Belfore<sup>1</sup>, Gandhari Bhandari<sup>1</sup>, Tyler J. Grassman<sup>2</sup>, Angus Rocketts<sup>3</sup>, and Sylvain Marsillac<sup>1</sup>

<sup>1</sup>Virginia Institute of Photovoltaics, Old Dominion University, Norfolk, VA 23529, USA

<sup>2</sup>Dept. of Materials Science & Engineering, The Ohio State University, Columbus, OH 43210, USA

<sup>3</sup>Dept. of Metallurgical and Materials Engineering, Colorado School of Mines, Golden, CO 80401, USA

**Abstract** — Solar cell degradation can occur through many pathways and at the different stages of the fabrication process, notably due to water condensation. In the case of Cu(In, Ga)Se<sub>2</sub> solar cells, the impact of water ingress on Mo back contact can be substantial, for not only the film itself but also the device performance and reliability. Micro-structural modification, change in film morphology, loss in reflectance, and increased resistivity due to moisture ingress were observed via X-ray diffraction, transmission electron microscopy, spectroscopic ellipsometry, and four-point probe measurements. Secondary ion mass spectrometry measurements revealed drastic changes in the alkali (Na, K) profiles in both the CIGS and Mo layers, likely due to a modification of their diffusion coefficient through Mo. This in turn negatively impacts the solar cell efficiency by decreasing both fill factor and open circuit voltage. Additional experiments, modifying the substrate and utilizing a NaF post-deposition treatment, highlight the mechanisms of degradation as being due to both a modification of the Mo/CIGS interface and the lack of alkali diffusion after water ingress.

**Index Terms** — Molybdenum, Cu(In, Ga)Se<sub>2</sub>, photovoltaic cells, semiconductor device reliability, stability, water ingress, degradation

## I. INTRODUCTION

Molybdenum thin films have been used for many years as the back contact for the fabrication of CuIn<sub>1-x</sub>Ga<sub>x</sub>Se<sub>2</sub> (CIGS) solar cells, and, to date, continue to be used in high-efficiency CIGS devices [1]. This material presents many advantages, including low contact resistance with CIGS layer, mechanical stability during high-temperature CIGS growth process, good adhesion with soda lime glass (SLG) substrate, viable pathways for Na diffusion from SLG, chemical inertness and formation of a beneficial MoSe<sub>2</sub> interfacial layer [2,3]. However, the susceptibility of Mo to degrade in a humid environment is a potential concern for the long-term stability of these solar cell devices [4, 5]. Many studies have therefore been conducted to investigate the effect of damp heat and moisture on the properties of Mo thin films [6-9]. Researchers have shown that the surface oxidation of Mo films results in the loss of both conductivity and reflectivity [10, 11], while it can also prevent the formation of a beneficial interfacial MoSe<sub>2</sub> [12]. Meanwhile, the effect of Mo oxidation on device performance is not completely consistent, as some researchers observed positive effects, while others have noticed negative effects [8,

13, 14]. Another related and critical degradation mechanism is due to water ingress or water condensation [15, 16], which can happen on fielded modules, but also at various stages of the fabrication process, especially for a batch process.

In this paper, Mo thin films exposed to deionized water (DIW) for 24 h at 50°C are studied to assess the failure mechanisms of Mo back contacts due to water ingress and to elucidate the impact of Mo degradation on the device performance. Several types of samples were prepared to allow for more accurate identification of the issues, and solutions are proposed to test and confirm our hypothesis.

## II. EXPERIMENTAL DETAILS

CIGS devices with a Mo/CIGS/CdS/i-ZnO/ITO structure were fabricated on SLG and alumina substrates. A Mo bilayer was deposited by DC magnetron sputtering at a constant power density of 7.4 W/cm<sup>2</sup>. The bottom layer was deposited at an Ar pressure of 1.33 Pa and the top layer at a lower pressure of 0.4 Pa. The resulting combined thickness of the Mo film was ~800 nm. For the CIGS deposition, Mo samples from the same batch were used. Half of the Mo samples were immersed into deionized water (18.2 MΩ) at 50°C for 24 h in a glass beaker prior to CIGS deposition (referred to as water-soaked (WS) samples), while the other half was kept in a desiccator. The CIGS layers (~2 micron) were thereafter deposited using a three-stage co-evaporation process [17] as reported in reference [18]. The cells were completed by depositing CdS (50-60 nm) using chemical bath deposition, i-ZnO (70-80 nm) and ITO (250-300 nm), both using RF sputtering with a constant power density of 4.9 W/cm<sup>2</sup> at Ar pressure of 0.67 Pa. Finally, the Ni/Al/Ni front contacts were deposited by e-beam evaporation. Table 1 summarizes the type of CIGS samples studied in this work. Sample A prepared on SLG substrate and Sample D prepared on alumina substrate are the reference samples in the experiment, allowing comparison with the water exposed samples.

The structural analysis of the films was done by X-ray diffraction (XRD) (Miniflex benchtop X-ray diffractometer, Rigaku) and the optical properties were extracted using spectroscopic ellipsometry (M2000, J.A. Woolam Co.). The cross-section morphology was studied by scanning transmission electron microscopy (STEM). Samples for STEM

work were prepared in a FEI Helios Ga-source focused ion beam (FIB) at 30 kV using low currents (48 pA - 96 pA) and finished with a 5 kV cleanup to minimize amorphous damage. STEM imaging was performed on an image-corrected FEI Titan3 G2 STEM at 300 kV. Secondary ion mass spectrometry (ToF SIMS) was used to measure the compositional variation as a function of depth in the device. ToF-SIMS analyses were conducted using a TOF SIMS V (ION TOF, Inc. Chestnut Ridge, NY) instrument. 3 keV Cs<sup>+</sup> with 20 nA current was used to create a 120 μm by 120 μm area, while a middle 50 μm by 50 μm area was analyzed using 0.3 pA Bi<sup>3+</sup> primary ion beam. The photovoltaic characteristics were evaluated by in-house current density-voltage (J-V) measurements under AM1.5G with a light intensity of 100 mW/cm<sup>2</sup> at 25°C (IV5, PV measurement Inc.) and by external quantum efficiency (QE) measurements (QEX7, PV measurement Inc.).

TABLE I  
SUMMARY OF THE CIGS SAMPLES USED IN THIS STUDY

Sample	Substrate	Mo WS	NaF PDT
A	SLG	No	No
B	SLG	Yes	No
C	SLG	Yes	Yes
D	Alumina	No	Yes
E	Alumina	Yes	Yes

### III. RESULTS AND DISCUSSION

#### A. Characterization of Mo on SLG substrate

The XRD diffractograms of the reference Mo and water-soaked Mo are shown in Fig. 1 (insert). The anticipated peaks relating to Mo-O phases were not evident in the symmetric geometry ( $\theta/\theta$ ) XRD patterns at least in the water-soaked Mo. Furthermore, no noticeable change in the peak position, intensity, or broadening was observed in the symmetric geometry XRD( $\theta/\theta$ ) patterns. However, glancing incidence XRD (GIXRD) patterns of Mo before and after water soaking, taken at an asymmetric geometry with 0.5° angle of incidence (probing primarily the surface region), shows a different trend. The (110), (200) and (211) peaks of Mo are observed in both films (note that the (200) peak is not readily observable in the XRD ( $\theta/\theta$ ) scans). The peak intensity of the (200) drastically diminished after water soaking, while the (110) and (211) intensities were only slightly reduced. It shows that, although [110] is the main crystal orientation of the Mo films, there are some changes in the orientation of the top Mo layer after water soaking.

The film structure and the electrical properties of the Mo film were optically analyzed by spectroscopic ellipsometry (SE) measurement before and after water soaking the Mo layer. Mo bulk layer plus the surface roughness layer on top was used as the nominal structural model used in the analysis of the SE data. The dielectric functions of the surface roughness layer were determined using the Bruggeman effective medium

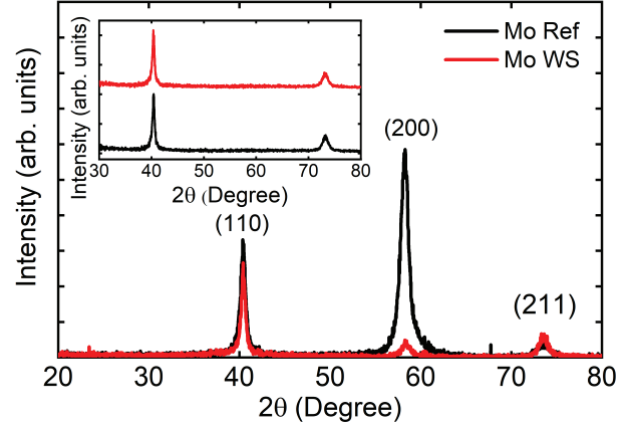


Fig. 1. GIXRD pattern of the reference Mo film and the water-soaked Mo film at 0.5° angle of incidence (insert: symmetric XRD pattern).

approximation (EMA) [19] by assuming a mixture of bulk layer material and voids (50% Mo - 50% voids). The complex dielectric functions ( $\epsilon$ ) of the Mo layers were obtained by mathematical inversion [20]. The parametric form of the extracted dielectric functions using a Drude oscillator ( $\epsilon_{Drude(RT)}$ ) [20] and three critical point parabolic band oscillators (CPPB) [20] expressed in equation (1), was obtained by least square regression analysis.

$$\epsilon(E) = \epsilon_{1,\infty} + \epsilon_{Drude(RT)} + \sum_{n=1}^3 \epsilon_{CPPB,n}(E) \quad (1)$$

where  $\epsilon_{1,\infty}$  is an energy-independent contribution to the real part of the dielectric function.

Fig. 2 shows the dielectric functions of the reference Mo and the water-soaked Mo. A rapid decrease in the  $\epsilon_1$  spectra below the photon energy of 1.5 eV, represents the dielectric response due to the free-carrier absorption related to the Drude term. The resistivity and the scattering time deduced from the Drude term suggest that the resistivity increased by  $\sim 2x$  and the scattering time decreased by  $\sim 2x$  after water soaking. The increase in resistivity as observed with ellipsometry correlated well with the measured resistivity from four-point probe measurements. The relatively short scattering time in the water exposed Mo may result from the increased grain boundary scattering [21]. It was also observed that the amplitude of  $\epsilon_2$  for the reference Mo was higher compared to the water-soaked Mo, which occurs due to the stronger optical absorption associated with the interband transitions [21]. This, in turn, suggests a higher void volume fraction or a decrease in the crystallite packing density of the water-soaked Mo compared to the reference Mo [21, 22]. It is worth noting here that the surface roughness layer from this analysis was found to increase from  $6.7 \pm 2$  nm to  $14 \pm 3$  nm after water soaking. The apparent increase in porosity or decrease in density of the Mo film after water exposure from this optical analysis was further validated by high-angle annular dark field (HAADF) STEM analysis discussed in the next section. Additionally, the reflectance of the Mo sample before

and after water exposure, as measured by spectroscopic ellipsometry (SE), is shown in Figure 2 (insert). The reflectance of the Mo samples dropped by  $\sim 50\%$  on average after water soaking in the measured wavelength range from 300 nm to 1000 nm.

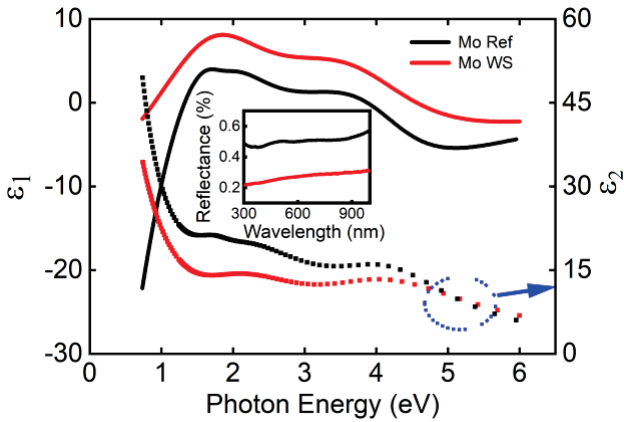


Fig. 2. Dielectric functions  $\mathcal{E} = \mathcal{E}_1 + i\mathcal{E}_2$  of the Mo films before and after water soaking. (Insert: reflectance versus wavelength for the reference and the water-soaked Mo film).

### B. Effects of Mo degradation on the CIGS films

Fig. 3a shows the HAADF STEM images of CIGS devices prepared on SLG/Mo substrates. The cross-sectional images reveal a significant change in the morphology of the water-soaked Mo film. The reference Mo shows a bilayer columnar grains as expected since the bottom layer was deposited at high Ar pressure and the top layer was deposited at low Ar pressure with a constant sputtering power density to obtain an adhesive high conductive film [23]. While the bottom layer of the water-soaked Mo resembled the reference Mo, the top layer was structurally degraded. This suggests a progressive degradation occurring from the top to the bottom part. Figure 3a also described the changes seen in the GIXRD pattern (Fig. 1). While the bottom Mo layer orientation did not change after water soaking, the top layer orientation has been changed, which is seen in the GIXRD analysis at  $0.5^\circ$  angle of incidence. Comparing the intensity in the HAADF STEM images reveals an interesting result. We note here that, for the same material, the contrast in the HAADF images depends on the local density of the material. In the case of the as-deposited Mo, the bottom layer appeared darker than the top layer, as expected since Mo deposited at low Ar pressure is denser than at high Ar pressure (other parameters remaining constant). However, in the water exposed Mo, the top layer appeared darker compared to the top layer of the reference Mo and was almost similar in contrast to the bottom Mo layer, indicating a lower density of the material. This is in close agreement with the spectroscopic ellipsometry results. The apparent lower density of degraded Mo may result from the additional contribution coming from Mo oxidation since the density of  $\text{MoO}_x$  is much lower than the density of Mo. To corroborate this argument, EDS analysis was performed

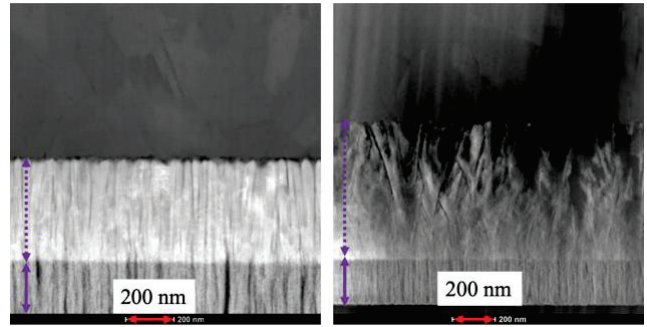


Fig.3a STEM-HAADF images of CIGS samples prepared on reference (left) and water-soaked Mo (right) (both on SLG substrate). The top and the bottom Mo layer in the images are distinguished by a solid and dotted line respectively. On top of Mo, a portion of the CIGS layer is seen in both images.

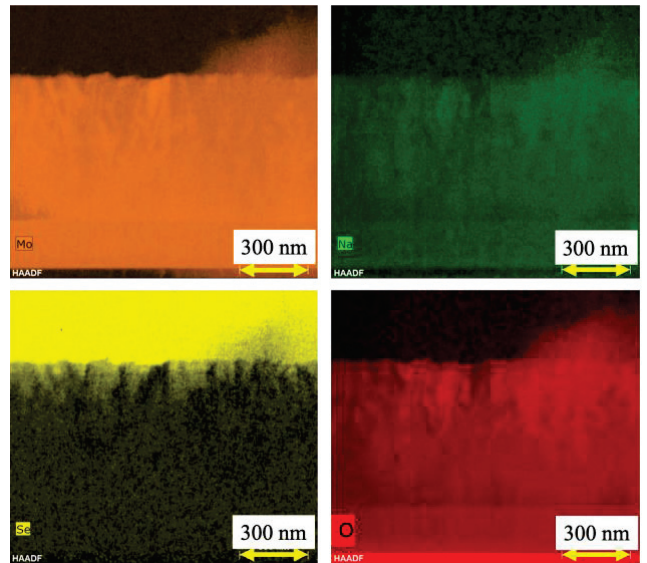


Fig. 3b. Elemental distribution of Mo, O, Se and Na in the water soaked Mo measured by EDS in STEM. The measurement was done after CIGS deposition (here on top, indicated by the intense Se signal).

and showed a higher concentration of oxygen at the top layer, indicating oxidation of Mo (see Fig. 3b).

Furthermore, the areas with higher oxygen content are associated with higher Na content as well, possibly due to the formation of a Na-containing Mo oxide such as  $\text{Na}_x\text{MoO}_3$  [14, 24] or formation of thermodynamically favorable  $\text{Na}_2\text{O}$  disrupting the Mo-O bonds [25]. Since the measurement was done on the sample after the CIGS deposition, Se was observed in the near-surface region of degraded Mo. Since there is an inverse correlation between Mo and Se contents, it is likely that Se diffused rather than merely forming a  $\text{MoSe}_2$  layer, which is also supported by the observation that  $\text{MoO}_2$  suppresses the formation of a  $\text{MoSe}_2$  layer [12]. It is possible that the selenium diffusion occurred through the micro-cracks in oxidized Mo whose surface roughness layer, composed of underlying Mo

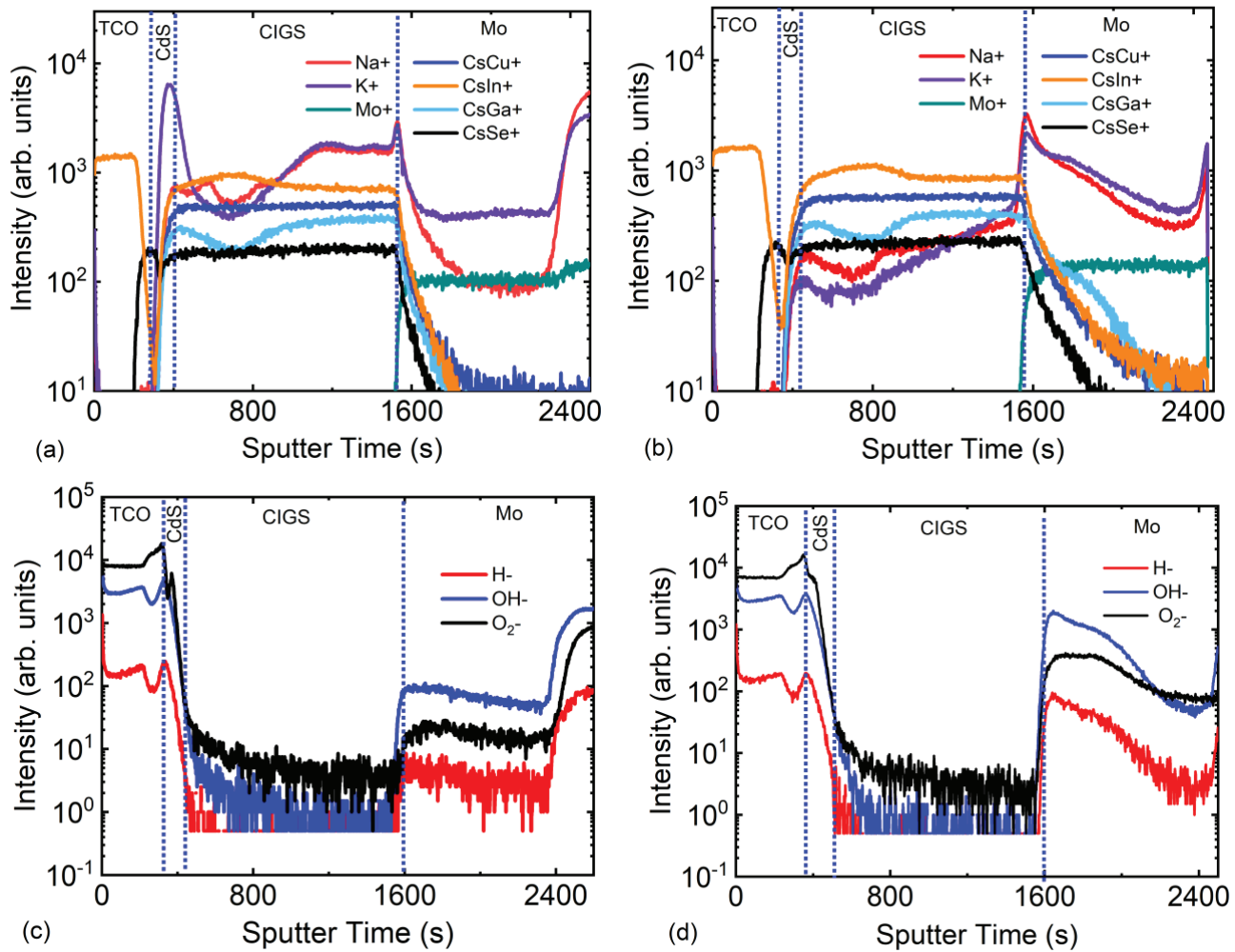


Fig. 4. Elemental distribution in the CIGS devices prepared on reference Mo (a – positive SIMS, c-negative SIMS) and water-soaked Mo (b-positive SIMS, d-negative SIMS) deposited on SLG substrates.

together with voids, was also found to be roughly twice as high as the reference Mo by SE analysis.

CIGS devices prepared on SLG substrates were analyzed by SIMS measurements (Fig. 4). Although purely quantitative analysis of the SIMS spectra could not be made due to lack of a standard, a comparative study of the elemental profiles can still be made. The Ga/(In+Ga) ratio for the CIGS on reference and water-soaked Mo showed no noticeable difference. Moreover, the overall composition of the CIGS film did not show a statistically significant difference. We can, therefore, assume that the constituent elemental profile of the CIGS film and the overall composition remains identical for both samples, as expected.

Of particular interest here is the distribution of alkali elements (Na, K) in the CIGS layer (Fig. 4(a, b)). It is well known that alkali ions diffuse during the CIGS growth from the SLG substrate into the CIGS through the intermediate Mo layer. The properties of the Mo layer are therefore of critical importance to the diffusion of the alkali into the CIGS. Here, the alkali

element profile has a rising trend within the bulk Mo when it is water-soaked but is relatively flat for the reference sample inside Mo layer. On the other hand, when deposited on WS Mo, going from the Mo/CIGS interface to the CIGS/CdS interface, the alkali element profile has a relatively steeper downward slope up to the Ga notch in the CIGS. Both alkali species track with the Ga profile exceedingly well in both samples. Furthermore, the bump in alkali ion counts at the CIGS/CdS interface observed in the reference sample is drastically reduced in the Mo WS sample.

Significant differences can also be seen in the negative SIMS profile (Fig. 4(c, d)). The H<sup>-</sup>, OH<sup>-</sup> and O<sub>2</sub><sup>-</sup> profiles in the reference samples are relatively flat in Mo while nearly absent in the CIGS. In the water-soaked Mo samples, all profiles slope upward from the glass substrate toward the CIGS. This is in good agreement with the oxidation observed by STEM/EDS. Another trend, also observed for the alkali profiles, is a clear demarcation between the top Mo layer (1600-2200 sec) and the

bottom Mo layer (2200-2500 sec) with a sharp increase in the Na signal in the reference Mo film however such demarcation is rarely visible in WS Mo. This can be also seen in Fig 3a, where the regular Mo has two clear layers (seen by a difference of contrast, related to a difference of density), while the WS Mo is much more uniform in terms of contrast.

Several previous studies have shown a higher diffusion of sodium in the Mo layer deposited at relatively higher Ar pressure, which is also evident here in the reference Mo when we compare the Na intensity level at the bottom part deposited at high pressure to the top part deposited at low Ar pressure [24, 26]. These variations in the sodium diffusion are linked to the oxygen content, which is believed to provide a chemical driving force for Na diffusion in Mo [24, 27]. However, simultaneous Na accumulation in oxidized Mo but frustrated diffusion into the subsequently prepared CIGS was seen in this experiment and elsewhere [14]. This suggests that the degree of oxidation in Mo back contact plays a vital role in alkali incorporation in the CIGS films, when entirely dependent on the Na supply from the SLG substrate. Based on our experimental results a possible explanation for the observed phenomena is that: (i) the oxidized Mo facilitates a higher diffusion of alkali within Mo; (ii) the interaction of adsorbed chemical species during CIGS deposition with the heavily modified surface of Mo (as seen by GIXRD, SIMS and SE) forms a barrier to the further diffusion, where there is a significantly thicker blocking layer at the Mo/CIGS interface. The modified alkali profile both in Mo (accumulation) and the CIGS (depletion) was simulated using COMSOL and correlated with previous studies of alkali diffusion in Mo [28]. Using similar COMSOL methodology, the oxidized Mo layer was determined to have a blocking layer twice as thick.

### C. CIGS Device Performance

The changes in alkali content in the CIGS observed in Fig. 4, can result in a significant loss in device performance [29, 30]. Solar cells were therefore fabricated according to Table I, to study the influence of Mo back contact on the device performance (Fig. 5). Fig. 5 shows a summary of the key photovoltaic parameters for the different types of devices and Fig. 6. shows representative dark J-V curves, with a double diode model fit for the same devices (labeled A to E) [31]. Compared to the reference device on SLG (Device A), the water-soaked Mo device (Device B) shows significant performance losses, due to a decrease in  $J_{sc}$ ,  $V_{oc}$ , and FF. Also, device B tends to show a slight rollover characteristic in the forward bias. A rollover effect is commonly observed in CIGS devices with low carrier concentration, mostly due to a lack of Na [32, 33] and has been associated with a Schottky barrier at the back contact. This behavior is consistent with the SIMS analysis discussed in the previous section and suggests that Na diffusion in the CIGS layer is reduced after water soaking. In order to identify if the Mo water-soaking degrades the solar cell performance just by suppressing the Na diffusion (or if other phenomena are involved), we performed a NaF post-deposition treatment (PDT) after the growth of CIGS on a device with a

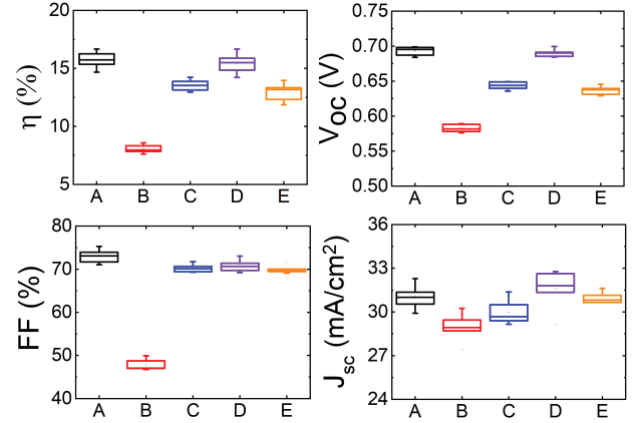


Fig. 5. Box plot of the CIGS devices (25 cells) parameters for all samples listed in Table I.

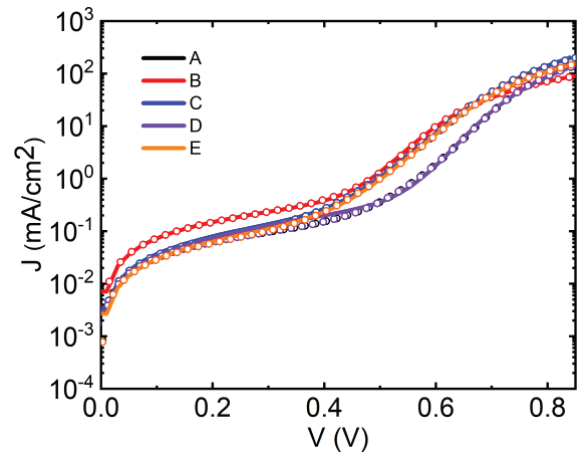


Fig. 6. Dark J-V characteristics (left) of a representative device with double diode model fit (symbols) from each category listed in Table I.

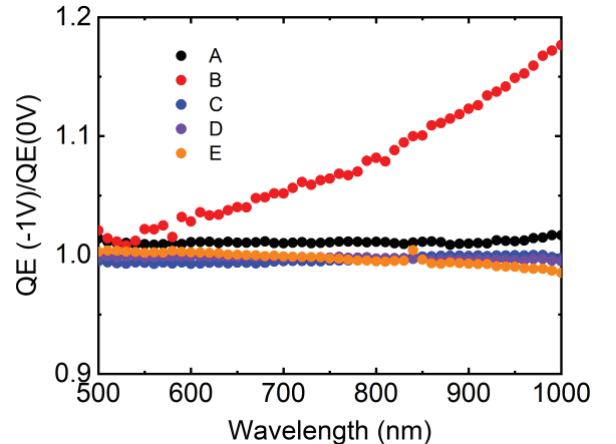


Fig. 7. The ratio of the quantum efficiency  $QE(-1V)/QE(0V)$  of the representative device from each category listed in Table I.

SLG/water-soaked Mo substrate (Device C). As shown by the device characteristics and the J-V curve, a partial recovery in the  $V_{oc}$ , FF, and  $J_{sc}$  was observed after the NaF PDT.

TABLE II  
PHOTOVOLTAIC CHARACTERISTICS AND DIODE PARAMETERS (DARK J-V) OF THE REPRESENTATIVE CELLS SHOWN IN FIG. 6.

Device ID	$\eta$ (%)	$V_{oc}$ (mV)	$J_{sc}$ (mA/cm <sup>2</sup> )	FF (%)	$J_{01}$ $\times 10^{-10}$ (mA/cm <sup>2</sup> )	$J_{02}$ $\times 10^{-05}$ (mA/cm <sup>2</sup> )	$R_s$ ( $\Omega$ .cm <sup>2</sup> )	$R_{sh}$ (k $\Omega$ .cm <sup>2</sup> )
A	16.5	697	31.4	75.5	0.25	1.17	0.73	3.26
B	8.6	576	29.5	50.7	111	4.08	2.34	1.37
C	13.6	657	29.2	70.9	0.87	5.32	0.66	2.89
D	16.0	699	31.4	73.0	0.24	1.16	0.93	3.20
E	13.9	646	30.2	71.5	1.21	4.91	0.96	3.52

Furthermore, no rollover was observed after NaF PDT. This indicates that other factors besides Na are in play for the performance drop. To further validate that the detrimental effect is due to more than a lack of Na diffusion, CIGS devices were grown on alkali-free alumina substrates. Devices D and E were prepared in the same CIGS batch with NaF PDT, but with a Mo water-soaked substrate for Device E and a reference Mo for Device D. Device performances for Device D were comparable to the reference Device A prepared on SLG glass (Fig. 5.), while Device E produced degraded devices comparable to Device C (SLG/WS Mo with NaF PDT). A double diode model was then used to extract the diode parameters of all the devices (Table II)[31]. One can see that the value of the reverse saturation current density,  $J_{01}$ , is order/s of magnitude higher in Devices B and E as compared to their respective reference Devices A and D. The device with the most degradation is Device B, with no NaF PDT, for which all diode parameters degrade rather significantly, including in  $R_s$  and  $R_{sh}$ .

Fig. 7. shows the  $QE(-1V)/QE(0V)$  ratio for devices A through E. Except for device B the ratio is close to 1, which indicates that there is no significant carrier collection loss in these samples. For device B, the ratio is wavelength dependent. The increased voltage-dependent carrier collection at longer wavelength suggests poor minority carrier collection on water-soaked Mo [34].

## VI. CONCLUSION

Device efficiency and reliability can change drastically when expose to harsh environments. The origins of these modifications can sometimes be difficult to ascertain due to the multiple effects that can occur on the materials properties. In the case of Cu(In,Ga)Se<sub>2</sub> solar cells, the exposure of the back contact to water ingress has an immediate effect on the Mo layer right after exposure, and an even stronger effect after Cu(In,Ga)Se<sub>2</sub> deposition. However, the most drastic effect occurs due to the modification of the alkali diffusion process from the substrate into the Cu(In,Ga)Se<sub>2</sub> layer. By varying the substrates and the origin of the alkali (applying post-deposition treatment), the distinction between the hindered alkali diffusion effect and the Mo/Cu(In,Ga)Se<sub>2</sub> interface effect were separated, demonstrated that both were present.

## ACKNOWLEDGEMENT

This research was supported by the Department of Energy Contract No. DE-EE0007141. We would like to thank Dr. D.W. Comb from The Ohio State University for his help on STEM analysis.

## REFERENCES

- [1] A. Freundlich, P. Verlinden, and W. van Sark, *Photovoltaic Solar Energy: From Fundamentals to Applications*. John Wiley & Sons, 2017.
- [2] S. Nishiwaki, N. Kohara, T. Negami, and T. Wada, "MoSe<sub>2</sub> layer formation at Cu (In, Ga)Se<sub>2</sub>/Mo Interfaces in High-Efficiency Cu (In<sub>1-x</sub>Ga<sub>x</sub>)Se<sub>2</sub> Solar Cells," *Japanese Journal of Applied Physics*, vol. 37, no. 1A, p. L71, 1998.
- [3] D. Abou-Ras *et al.*, "Formation and characterization of MoSe<sub>2</sub> for Cu(In,Ga)Se<sub>2</sub> based solar cells," *Thin Solid Films*, vol. 480–481, pp. 433-438, 6/1/ 2005.
- [4] J. Wennerberg, J. Kessler, L. Stolt, "Cu (In,Ga)Se<sub>2</sub>-based thin-film photovoltaic modules optimized for long-term performance," *Solar Energy Materials and Solar Cells*, vol. 75, no. 1-2, pp. 47-55, 2003.
- [5] T. J. McMahon, "Accelerated testing and failure of thin-film PV modules," *Prog. Photovolt: Res. Appl.* vol. 12, no. 2 - 3, pp. 235-248, 2004.
- [6] M. Theelen and F. Daume, "Stability of Cu (In, Ga) Se<sub>2</sub> solar cells: A literature review," *Solar Energy*, vol. 133, pp. 586-627, 2016.
- [7] J. Pern and R. Noufi, "An investigation of stability issues of ZnO and Mo on glass substrates for cigs solar cells upon accelerated weathering and damp heat exposures," in *DOE SETP Review Meeting, Denver, CO*, 2007, vol. 4, pp. 17-19.
- [8] P. M. Salomé, V. Fjallstrom, A. Hultqvist, P. Szaniawski, U. Zimmermann, and M. Edoff, "The effect of Mo back contact aging on Cu (In, Ga) Se<sub>2</sub> thin - film solar cells," *Progress in Photovoltaics: Research and Applications*, vol. 22, no. 1, pp. 83-89, 2014.

- [9] M. Theelen *et al.*, "Influence of Mo/MoSe<sub>2</sub> microstructure on the damp heat stability of the Cu (In, Ga) Se<sub>2</sub> back contact molybdenum," *Thin Solid Films*, vol. 612, pp. 381-392, 2016.
- [10] M. Theelen, F. d. Graaf, F. Daume, N. Barreau, Z. Vroon, and M. Zeman, "Damp heat-related degradation mechanisms within CIGS solar cells," in *2016 IEEE 43rd Photovoltaic Specialists Conference (PVSC)*, 2016, pp. 2292-2297.
- [11] R. Feist *et al.*, "Examination of lifetime-limiting failure mechanisms in CIGSS-based PV minimodules under environmental stress," in *33rd IEEE Photovoltaic Specialists Conference*, 2008, pp. 1-5.
- [12] A. Duchatelet, G. Savidand, R. N. Vannier, and D. Lincot, "Optimization of MoSe<sub>2</sub> formation for Cu(In,Ga)Se<sub>2</sub>-based solar cells by using thin superficial molybdenum oxide barrier layers," *Thin Solid Films*, vol. 545, pp. 94-99, 10/31/ 2013.
- [13] Y. Kamikawa, J. Nishinaga, S. Ishizuka, H. Shibata, and S. Niki, "Effects of Mo surface oxidation on Cu (In, Ga) Se<sub>2</sub> solar cells fabricated by three-stage process with KF postdeposition treatment," *Japanese Journal of Applied Physics*, vol. 55, no. 2, p. 022304, 2016.
- [14] S. Lin *et al.*, "Adjustment of alkali element incorporations in Cu (In, Ga) Se<sub>2</sub> thin films with wet chemistry Mo oxide as a hosting reservoir," *Solar Energy Materials and Solar Cells*, vol. 174, pp. 16-24, 2018.
- [15] N. Park, C. Han, and D. J. M. R. Kim, "Effect of moisture condensation on long-term reliability of crystalline silicon photovoltaic modules," *Microelectronics Reliability*, vol. 53, no. 12, pp. 1922-1926, 2013.
- [16] M. D. Kempe, "Modeling of rates of moisture ingress into photovoltaic modules," *Solar Energy Materials and Solar Cells*, vol. 90, no. 16, pp. 2720-2738, 2006.
- [17] R. Noufi *et al.*, "Method of fabricating high-efficiency Cu(In, Ga)(SeS)<sub>2</sub> thin films for solar cells," ed: Google Patents, 1995.
- [18] S. Karki *et al.*, "In Situ and Ex Situ Investigations of KF Postdeposition Treatment Effects on CIGS Solar Cells," *IEEE Journal of Photovoltaics*, vol. 7, no. 2, pp. 665-669, 2017.
- [19] D. Abou-Ras, T. Kirchartz, and U. Rau, *Advanced Characterization Techniques for Thin Film Solar Cells*. Wiley, 2016.
- [20] H. Fujiwara, *Spectroscopic Ellipsometry: Principles and Applications*. Wiley, 2007.
- [21] J. Walker, H. Khatri, V. Ranjan, J. Li, R. Collins, and S. Marsillac, "Electronic and structural properties of molybdenum thin films as determined by real-time spectroscopic ellipsometry," *Applied Physics Letters*, vol. 94, no. 14, p. 141908, 2009.
- [22] J. Li *et al.*, "Density profiles in sputtered molybdenum thin films and their effects on sodium diffusion in Cu (In<sub>x</sub>,Ga<sub>1-x</sub>)Se<sub>2</sub> photovoltaics," in *2011 37th IEEE Photovoltaic Specialists Conference*, 2011, pp. 002749-002752: IEEE.
- [23] H. A. Al-Thani *et al.*, "The effect of Mo back contact on Na out-diffusion and device performance of Mo/Cu (In,Ga)Se<sub>2</sub>/CdS/ZnO solar cells," in *Conference Record of the Twenty-Ninth IEEE Photovoltaic Specialists Conference, 2002.*, 2002, pp. 720-723: IEEE.
- [24] J.H. Yoon, T.Y. Seong, and J.H. Jeong, "Effect of a Mo back contact on Na diffusion in CIGS thin film solar cells," *Progress in Photovoltaics: Research and Applications*, vol. 21, no. 1, pp. 58-63, 2013.
- [25] G. K. Rane, S. Menzel, T. Gemming, and J. Eckert, "Microstructure, electrical resistivity and stresses in sputter deposited W and Mo films and the influence of the interface on bilayer properties," *Thin Solid Films*, vol. 571, pp. 1-8, 2014.
- [26] M. Bodegård, K. Granath, L. Stolt, A. Rockett, "The behavior of Na implanted into Mo thin films during annealing," *Solar Energy Materials and Solar Cells*, vol. 58, no. 2, pp. 199-208, 1999.
- [27] R. V. Forest, E. Eser, B. E. McCandless, R. W. Birkmire, and J. G. Chen, "Understanding the role of oxygen in the segregation of sodium at the surface of molybdenum coated soda-lime glass," *AIChE Journal*, vol. 60, no. 6, pp. 2365-2372, 2014.
- [28] B. Belfore, O. Ayala, T. Ashrafee, G. Rajan, S. Karki, and S. Marsillac, "Modeling Diffusion of Impurities in Molybdenum Thin Films as a Function of Substrate Temperature," *IEEE Journal of Photovoltaics*, vol. 9, no. 1, pp. 339-343, 2019.
- [29] D. Rudmann *et al.*, "Efficiency enhancement of Cu(In, Ga)Se<sub>2</sub> solar cells due to post-deposition Na incorporation," *Applied Physics Letters*, vol. 84, no. 7, pp. 1129-1131, 2004.
- [30] P. Salom, V. Fjallstrom, A. Hultqvist, and M. Edoff, "Na Doping of CIGS Solar Cells Using Low Sodium-Doped Mo Layer," *IEEE Journal of Photovoltaics*, vol. 3, no. 1, pp. 509-513, 2013.
- [31] S. Suckow, "2/3-Diode Fit," ed, 2014.
- [32] D. Rudmann, "Effects of sodium on growth and properties of Cu(In,Ga)Se<sub>2</sub> thin films and solar cells," *Thesis ETH Zurich*, 2004.
- [33] J. M. Raguse, C. P. Muzzillo, J. R. Sites, and L. Mansfield, "Effects of Sodium and Potassium on the Photovoltaic Performance of CIGS Solar Cells," *IEEE Journal of Photovoltaics*, vol. 7, no. 1, pp. 303-306, 2017.
- [34] S. Hegedus, W.N. Shafarman, "Thin-Film Solar Cells: Device Measurements and Analysis" *Prog. Photovolt: Res. Appl.* 2004; 12:155–176 (DOI: 10.1002/pip.518)